Laser Trapping of Colloidal Metal Nanoparticles

Anni Lehmuskero,[†] Peter Johansson,[†,‡] Halina Rubinsztein-Dunlop,[§] Lianming Tong,[*,∥,⊥] and Mikael Käll[*,†]

[†]Department of Applied Physics, Chalmers University of Technology, 412 96 Göteborg, Sweden, [‡]School of Science and Technology, Örebro University, 701 82 Örebro, Sweden, [§]Quantum Science Laboratory, School of Mathematics and Physics, The University of Queensland, St. Lucia, Brisbane, Queensland 4072, Australia, [∥]Center for Nanochemistry, Beijing Science and Engineering Center for Nanocarbons, College of Chemistry and Molecular Engineering, Peking University, Beijing 100871, China, and [⊥]Beijing National Laboratory for Condensed Matter Physics and Institute of Physics, Chinese Academy of Sciences, Beijing 100190, China

ABSTRACT Optical trapping using focused laser beams (laser tweezers) has been proven to be extremely useful for contactless manipulation of a variety of small objects, including biological cells, organelles within cells, and a wide range of other dielectric micro- and nano-objects. Colloidal metal nanoparticles have drawn increasing attention in the field of optical trapping because of their unique interactions with electromagnetic radiation, caused by surface plasmon resonance effects, enabling a large number of nano-optical applications of high current interest. Here we try to give a comprehensive overview of the field of laser trapping and manipulation of metal nanoparticles based on results reported in the recent literature. We also discuss and describe the fundamentals of optical forces in the context of plasmonic nanoparticles, including effects of polarization, optical angular momentum, and laser heating effects, as well as the various techniques that have been used to trap and manipulate metal nanoparticles. We conclude by suggesting possible directions for future research.

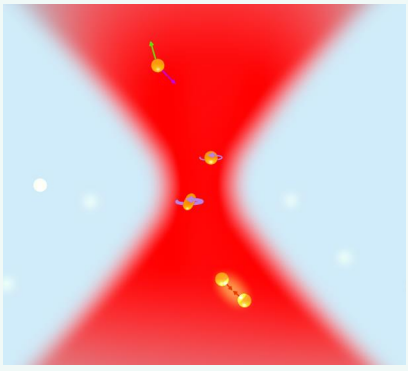

KEYWORDS: laser tweezers · optical manipulation · optical force · optical torque · colloidal metal nanoparticles · surface plasmon resonance · interparticle forces · laser heating

The concept of optical trapping dates back to 1970 when Arthur Ashkin demonstrated that micron-sized dielectric particles could be accelerated and trapped in stable optical potentials produced by counter-propagating laser beams.[1] Subsequently, a single tightly focused laser beam, now known as laser tweezers, was used to trap dielectric microparticles, thus demonstrating that the so-called optical gradient force, under certain circumstances, can overcome the radiation pressure and lead to a stable optical trap in three dimensions (3D).[2] Laser tweezers and related optical trapping techniques have since been extensively studied and developed as powerful tools for manipulation of particles and for quantitative measurements of forces, positions, and torques in a broad range of multidisciplinary sciences ranging from atomic physics to cell biology. For relevant reviews, see references 3–7.

Common sense might suggest that it is impossible to trap a metallic object using laser tweezers since the refraction that is the basis for optical trapping of dielectric particles in the simplified ray-optics description of optical forces is absent: light is reflected back at the metal surface, which leads to a large radiation pressure, but the reflected light cannot generate an optical gradient force in the way that the refracted light in dielectric particles does. However, in 1994, Svoboda and Block experimentally demonstrated that this picture is misleading when one considers particles that are much smaller than the incident laser wavelength: subwavelength metal particles can indeed be stably trapped in 3D, and the trapping forces can even be substantially enhanced compared to dielectric particles of the same size.[8] This finding spurred an increasing interest in optical forces and laser manipulation of metal nanoparticles, an interest that has accelerated recently because of rapid developments in colloid synthesis methods, plasmonics, and nano-optics.

The interaction between light and metal nanoparticles is dominated by the coupling between the electric component of

* Address correspondence to lianming.tong@pku.edu.cn, mikael.kall@chalmers.se.

Received for review January 14, 2015 and accepted March 25, 2015.

Published online March 25, 2015
10.1021/acsnano.5b00286

the electromagnetic field and collective resonant oscillations of the metal conduction electrons known as localized surface plasmons (LSPs).[9] In the visible and near-infrared wavelength range, gold and silver nanoparticles show the strongest LSPs by far, but many other metals also exhibit pronounced plasmonic effects. The number of distinct LSPs that a particle supports, their resonance wavelength, charge displacement character, and damping characteristics, can be precisely tuned *via* the particle properties, in particular, by selecting the particle shape, size, and composition, but also *via* interparticle interactions and through the refractive index of the surrounding medium. Illumination of plasmonic nanoparticles with light in resonance with a LSP may lead to strongly enhanced light absorption (therefore effective light-to-heat conversion) and intense elastic (Rayleigh) light scattering, which together determine the color of the particle. Moreover, plasmon excitation induces strongly amplified optical near-fields near the metal surface, which means that plasmonic nanoparticles can be used as antennas that effectively couple in or out light to or from molecules, quantum dots, or other nanoscale objects.[10−12]

The peculiar optical properties of metal nanoparticles are a key ingredient in a variety of emergent nanoscience applications of great contemporary interest, including but not limited to a novel solar light-harvesting systems,[13−15] a range of molecular analysis and sensing methods,[16,17] exotic metamaterials,[18] and new nanophotonics solutions.[19,20] These properties are also what make metal nanoparticles interesting from the point of view of optical forces and manipulation. The early work of Ashkin suggested that optical forces could be enhanced by tuning the laser wavelength to specific optical transitions, thereby enabling laser trapping of atoms and molecules.[3] Similarly, the large and highly wavelength-dependent polarizability of a resonant metal particle can strongly enhance the optical force generated by a laser beam and even change the direction of the force. However, the large scattering and absorption cross sections associated with LSP excitation also lead to a large radiation pressure and to particle heating. These and related effects are of fundamental interest but can also lead to many captivating new applications.

This review aims to give a comprehensive summary of laser tweezers and manipulation studies of plasmonic nanoparticles in solution. We focus on metal colloids because almost all experimental studies in the field to date deal with colloids and because the rapid advances in colloid chemistry over the past decade(s) have resulted in the development of a wide range of exotic metal nanostructures (see, for example, ref 21 for a comprehensive review), including nanowires, nanorods, core−shell particles, nanoprisms, nanocubes, *etc.*, of which only a few have so far been explored in the context of optical forces and laser manipulation.[22−25]

VOCABULARY: laser tweezers – an optical means to trap and manipulate micro/nanoscale objects using a highly focused laser beam; **optical force** – a force induced by light *via* interaction with matter, specifically, through exchange and conservation of photon momentum; **colloidal metal nanoparticles** – chemically synthesized metallic nanoparticles, typically encapsulated by ions and stably suspended in solution due to electrostatic repulsion; **surface plasmons** – collective oscillations of conduction electrons in metal surface or metal nanostructure; **optical manipulation** – the mechanical manipulation of particles by light, such as trapping, movement, fixation, and rotation, using optical forces and optical torques

This paper represents a complementary review to several excellent recent ones on optical manipulation of nanostructures, in particular, the work of Dienerowitz *et al.*,[5] Maragò *et al.*,[26] and Bendix et al.,[27] who summarized results from a wide range of topics, and Urban *et al.*,[28] who described some fundamentals and applications of optical manipulation of plasmonic nanoparticles with an emphasis on work performed in the Feldmann group. Maragò *et al.*[26] also summarized important work on "plasmonics tweezers", that is, surface-supported plasmonic nanostructures used to enhance gradient forces for optical trapping of small objects in two dimensions (2D).[29]

We start by a description and discussion of the fundamentals of optical forces and torques (illustrated in Figure 1) based on the point dipole approximation as well as more realistic electrodynamics simulations. We continue with a brief summary of how to measure and characterize these forces in practice and then describe some of the laser tweezers techniques that have been used to trap colloidal metal nanoparticles in solution. The remaining part of the paper focuses on a few selected topics that we believe are of high current interest, including optical rotation experiments, optical aggregation, and applications in surface-enhanced Raman scattering (SERS), optical manipulation of metal colloids as a means for nanoscale lithography, and applications based on laser heating of optically trapped nanoparticles. We conclude by suggesting some possible avenues for further investigations.

THEORETICAL BACKGROUND

General Considerations. The force exerted on an object held in optical tweezers is ultimately due to conservation of the linear and angular momentum carried by the photons that the object absorbs or scatters from the incident light field. This notion is captured in the most general method for calculating optical forces, that is, by integrating the momentum flow, described by Maxwell's stress tensor, $\boldsymbol{T}$, over an arbitrary surface A enclosing the particle according to

$$\langle \mathbf{F} \rangle = \oint\oint \langle \boldsymbol{T} \rangle \cdot \mathbf{n} \mathrm{d}A \qquad (1)$$

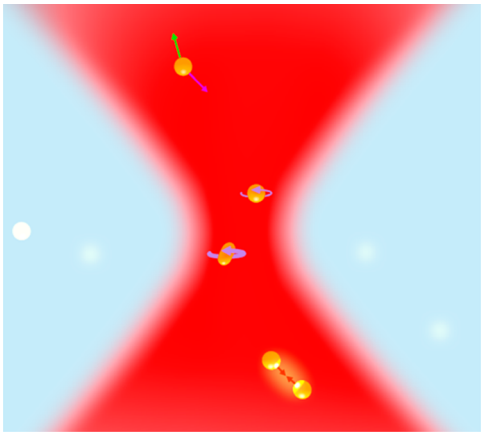

Figure 1. Illustration of important forces that influence the movement of metal colloids in a focused laser beam. The light exerts force through polarization and wavelength-dependent transfer of linear and/or angular photon momentum, resulting in optical gradient forces (purple arrow), radiation pressure (scattering + absorption forces, green arrow), and optical torques (rotation and spinning, rotational arrows). Optical forces can also be induced between particles through mutually scattered fields (red arrows). Light absorption leads to a temperature rise of the particle and the liquid surrounding it. This can in turn increase the amplitude of stochastic thermal forces, causing increased Brownian motion, and results in a decrease in the viscosity of the liquid, thereby decreasing friction and drag forces.

Here, the brackets denote a time average, **n** is a surface normal, and $\boldsymbol{T}$ can be calculated from the total electric and magnetic fields at the surface A. The stress tensor formalism is well-adapted to computational electromagnetic approaches, based on, for example, Mie theory or finite difference time domain simulations, and it is the method of choice for obtaining accurate quantitative estimates of optical forces. However, the physical background of optical trapping may be understood *qualitatively* from simplifying approximations, one or the other being more appropriate depending on the particle material (dielectric or metallic) and the particle size compared to the wavelength of the trapping light.[4,5] The ray-optics description of optical forces is based on the picture that light rays are refracted inside dielectric particles that are substantially larger than the wavelength. The refracted rays redirect the photon momentum, resulting in recoil that draws the particle toward the higher photon flux near the laser focus.[30] Unfortunately, this simple picture is not easily adapted to metal nanoparticles, which are subwavelength and strongly scatter and absorb the incident light. Instead, it is customary to use the so-called point dipole approximation, that is, to treat the particle as a point-like polarizable object that is acted upon by the incident field through the Lorentz force. Below, we briefly outline this approach and then use it to interpret full electrodynamics calculations of spherical gold particles residing in a focused laser field. We use SI units throughout.

Point Dipole Approximation. We assume that the particle is completely characterized by its electric dipole polarizability tensor $\boldsymbol{\alpha}$. The polarizability is determined by the particle shape and volume V, by the frequency-dependent dielectric response $\varepsilon(\omega)$ of the material of which the particle is made, and by the refractive index n_m of the surrounding medium. The incident electric field, $\boldsymbol{E}$, polarizes the particle in proportion to its polarizability and the resulting oscillating-induced dipole moment $\boldsymbol{p} = n_m^2\boldsymbol{\alpha E}$ is in turn acted upon by the field through the Lorentz force, causing the particle to move and/or rotate. In the simple case of a plane wave, this analysis leads to the conclusion that the optical force can be decomposed into two distinct components, the gradient force and the radiation pressure (or scattering−absorption) force. If we further assume that the particle has a spherical shape and therefore an isotropic (scalar) polarizability α, the force components take the form

$$\boldsymbol{F}_{\mathrm{grad}}(\boldsymbol{r}) = \frac{1}{2\varepsilon_0}Re\{\alpha\}\nabla I(\boldsymbol{r});\quad \boldsymbol{F}_{\mathrm{rp}}(\boldsymbol{r}) = \frac{n_m}{c}\sigma_{\mathrm{ext}}\langle \boldsymbol{S}(\boldsymbol{r})\rangle \quad (2)$$

Here $I(\boldsymbol{r})$ is the laser intensity at position $\boldsymbol{r}$, c is the speed of light in vacuum, $\boldsymbol{S}(\boldsymbol{r})$ is the Poynting vector, brackets $\langle\rangle$ denote time averaging, and for sufficiently small particles that scatter light in a dipole pattern, the particle extinction cross section $\sigma_{\mathrm{ext}} = \sigma_{\mathrm{abs}} + \sigma_{\mathrm{scat}}$ sets the radiation pressure. The absorption and scattering cross sections that contribute to the extinction cross section are determined through the polarizability by

$$\sigma_{\mathrm{scat}} = \frac{\omega^4 n_m^4}{6\pi c^4 \varepsilon_0^2}|\alpha|^2;\quad \sigma_{\mathrm{abs}} = \frac{\omega n_m}{c\varepsilon_0}\mathrm{Im}\{\alpha\} \quad (3)$$

In the case of a small spherical particle, the polarizability can be expressed as $\alpha(\omega) = 3V\varepsilon_0 \times (\varepsilon(\omega) - n_m^2)/(\varepsilon(\omega) + 2n_m^2)$, where V is the particle volume, $\varepsilon(\omega)$ the dielectric function of the nanoparticle material, and n_m the refractive index of the surrounding medium. The gradient force, which has a component in both the axial and lateral directions in an optical trap, is responsible for confining the particle into the trap. It is typically directed toward the high-intensity region. For a plasmonic particle, however, the change in phase of the dipole oscillation with respect to the incident field around the LSP resonance may result in a change of sign of the polarizability, such that the gradient force is attractive and highly enhanced on the low-frequency (red) side of the resonance but repulsive on the high-frequency (blue) side.[31−35] Hence, the strength and direction of the gradient force depends in a crucial way on the spectral position of the LSP with respect to the trapping laser wavelength. The radiation pressure, on the other hand, always propels the particles in the direction of the light energy flux, that is, in the direction of the Poynting vector. It is worth noting that an additional term contributing to the scattering force, arising from the curl of the spin angular momentum in

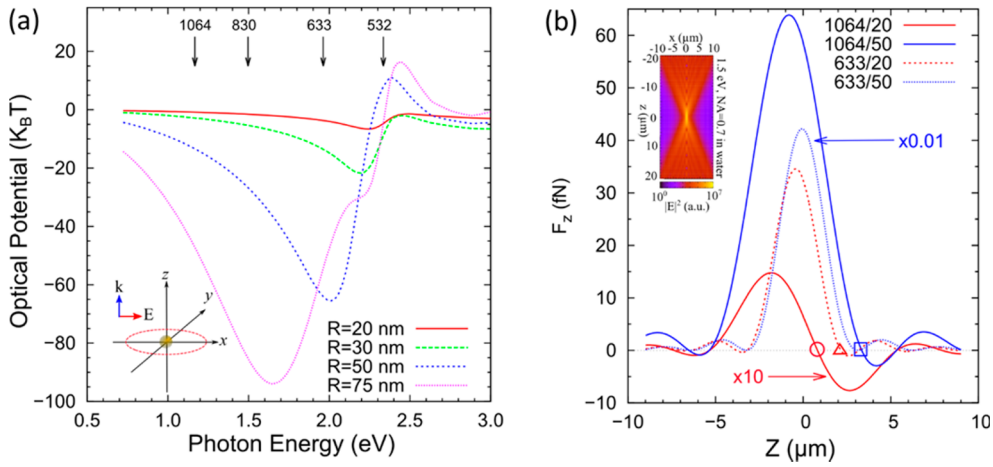

Figure 2. Results of electrodynamics calculations of optical forces acting on spherical gold particles in a focused laser beam with an intensity of 10 mW. (a) Calculated lateral optical potential at room temperature for gold nanoparticles of different radii *R* as a function of incident photon energy. The particle is located in water at the origin of the coordinate system, defined in the inset, and the field mimics an unpolarized laser beam focused by an NA = 0.7 objective. The arrows indicate some commonly employed laser wavelengths. (b) Axial optical forces acting on gold nanoparticles with radii *R* = 20 and 50 nm for two laser wavelengths, 1064 and 633 nm (note the different scale factors for the different cases). The inset shows the calculated beam profile.

a light field with nonuniform helicity, has been theoretically predicted.[36,37] Although the implications of this "curl force" are not yet completely clear, it can probably be safely neglected in the case of conventional trapping schemes.

Example of Electrodynamics Calculations. Figure 2 shows results of electrodynamics calculations of optical forces acting on gold particles of radii *R* = 20, 30, 50, and 75 nm residing in a focused laser beam as a function of photon energy. The calculations are based on an angular spectrum representation, containing only the propagating components, of a focused laser beam.[38] Hence, unlike the fields obtained from the so-called paraxial approximation, the fields impinging on the nanoparticle in this case are exact solutions of Maxwell's equations and can be projected onto vector spherical harmonics and expanded in terms of electric and magnetic multipole fields at the nanoparticle surface.[39] The projection is carried out by a numerical integration here. The force on the particle can then be calculated within the framework of Mie theory, with the aid of the Wigner–Eckart theorem.[40,41] We stress that these calculations take into account retardation effects and multipolar excitations that become more and more important with increasing particle size and that are not captured by the point dipole model, which is strictly only valid for particles of sizes much smaller than the laser wavelength. Figure 2a presents results related to the lateral component of the gradient force (*i.e.*, perpendicular to the light propagation direction). The 3D optical force field acting on the particle is not conservative, but by constraining the motion of the particle to one dimension (in this case the *x*-axis), we can introduce an optical potential energy defined as the work done by the optical force when the particle is brought from the origin to a distant point where the field vanishes. The figure shows the depth of the potential well (expressed in units of k_BT at room temperature) at the center of the focal plane of a Gaussian beam with a divergence that is set to mimic that produced by a microscope objective with numerical aperture NA = 0.7, which the authors have used in several experiments.[25,42−44] In water, this NA corresponds to a beam of convergence angle θ equal to 31.8°, that is, NA = n_{water} sin(θ) = 0.7. The excitation configuration and the calculated beam profile are shown in the insets of Figure 2a,b, respectively. The laser power is set to 10 mW, and commonly used laser lines are indicated by arrows.

The plasmonic responses of the gold particles are manifested as deep minima in the potential energy curves at the positions of the corresponding LSP resonances. The potential well deepens as the particle volume increases, in accordance with expectations from the point dipole model, while the red shift and broadening are due to finite size effects that are not taken into account in this first approximation. For the larger particles, one can also clearly see an antibinding effect at higher photon energies, signaling the aforementioned sign change of the particle dipole polarizability and the repulsive nature of the gradient force for photon energies slightly larger than the LSP resonance. For stable trapping in 3D, one also has to consider the forces along the optical axis, including both the gradient force and the radiation pressure. Figure 2b shows the net axial forces at different positions along the *z*-axis for particles of radii 20 and 50 nm for the 633 and 1064 nm laser lines, respectively. For the 1064 nm case, the force experienced by the 20 nm particle (red solid curve) is nearly antisymmetric around *z* = 0. In this case,

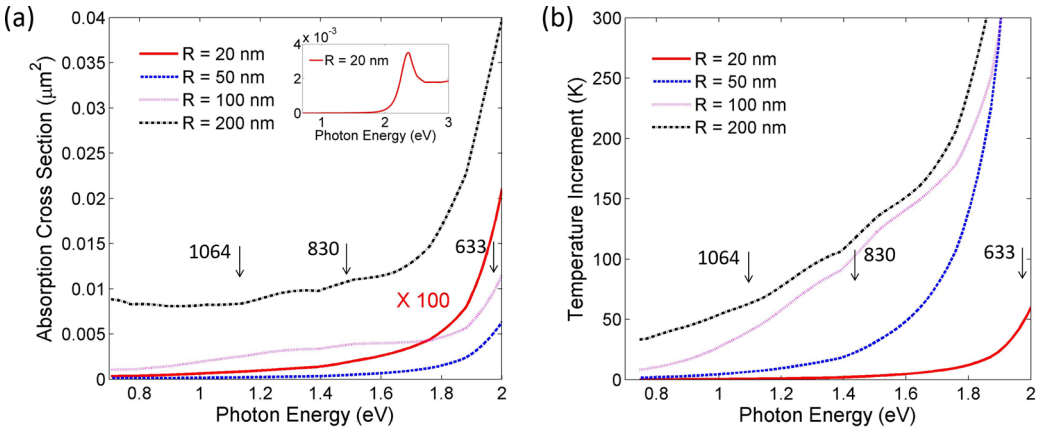

Figure 3. (a) Absorption cross sections of gold nanoparticles with radii of 20, 50, 100, and 200 nm (note the different scales for R = 20 nm) calculated from Mie theory. (b) Temperature increment of a gold nanoparticle at the focus of a 10 mW laser beam focused by an NA = 0.7 objective in water calculated by balancing the laser heating power and the power lost by heat conduction through the surrounding water. The arrows indicate some commonly employed laser lines.

the gradient force dominates over the radiation pressure, and there is an equilibrium position at $z \approx 1$ μm (highlighted by the red circle). Note that the equilibrium position is highly dependent on the NA of the objective and can be closer to the focal plane if the NA is higher. The larger R = 50 nm particle (blue solid curve) can also be trapped (at near z = 3.5 μm, blue square). However, for the 633 nm case, it is difficult to trap any particle because the laser frequency almost coincides with the LSP resonance, yielding a large polarizability α and consequently a higher radiation pressure. Also the ω^4 prefactor in eq 3 contributes to the rapid increase in radiation pressure with increasing photon energy. Several equilibrium positions due to multiple intensity maxima caused by diffraction effects are seen (for example, the one marked by the red triangle), but the corresponding restoring forces are weak and the trap is therefore unstable against thermal fluctuations in the axial direction. Note that the trends with wavelength and particle size seen in Figure 2 will be similar for other beam convergence angles, for example, corresponding to high NA immersion objectives, although the exact potential depths and force components will be different.

Heating Effects. Since metal nanoparticles have a large absorption cross section, heating can be pronounced and greatly affect the trapping stability by increasing Brownian thermal motion. This effect is theoretically considered in Figure 3. Figure 3a shows the calculated absorption cross section of gold nanoparticles with radii of 20, 50, 100, and 200 nm in water as a function of incident photon energy. We limit the attention to photon energies lower than the onset of interband transitions in gold, where the absorption cross section only varies weakly with photon energy up to the point where interband transitions set in and a sharp rise in absorption occurs. The inset in Figure 3a shows the resonance of a R = 20 nm particle. Small peaks are still observable at low photon energies for particles of radius R > 50 nm due to resonance effects. In Figure 3b, the temperature elevation compared to the room temperature is calculated for the same particles as in Figure 3a. Again, the laser power is 10 mW, and an objective of NA = 0.7 is used. The calculations assume homogeneous heating of the particle and a balance between the power absorbed by the particle and the power lost due to heat conduction through the water, which yields the temperature increment $\Delta T = P_{abs}/(4\pi R\kappa)$, where P_{abs} is the absorbed power, R the particle radius, and κ the thermal conductivity of water.[45] We see that the temperature increase is significant, particularly for the 633 nm laser case. It should be pointed out that, while it is likely that water close to the particle may be superheated, the highest temperatures reached here are not realistic. Nevertheless, even for the NIR laser lines commonly used for optical trapping, the heating effect should be considered with care in the explanation of experimental phenomena. Relevant experimental demonstrations will be discussed in the last section in this review.

Optical Torques. Photons can carry both intrinsic (spin) angular momentum, related to the circular polarization of the light, and, in the case of laser beams with a more complicated internal structure, also orbital angular momentum. Spin angular momentum can be transferred to mechanical angular momentum of an object, either by absorption of the photon or by scattering events that change the photon angular momentum. Such scattering events occur in the case where the particle is birefringent or has an anisotropic polarizability, as is the case for essentially any nonspherical particle. For example, nanorods, in general, have higher polarizability in the direction of the long axis than along the short axis. The time-averaged optical potential energy of the particle may then be written

$$U = -\langle \boldsymbol{p}\cdot\boldsymbol{E}\rangle = -\frac{n_m^2}{2}\sum Re\{\alpha_{ii}\}|E_i|^2,\ i = x,y,z \quad (4)$$

assuming a diagonal polarizability tensor, where $\boldsymbol{p}$ is the induced dipole moment.

Equation 4 shows that the optical potential depends on the direction of the electric field with respect to the particle orientation. For low photon energies, the potential energy is normally minimized when the particle's long axis is aligned with the electric field. At higher photon energies, other alignments are possible depending on the exact frequency dependence of the different elements of α. In general, the time-averaged torque τ that can be expressed by

$$\tau = \langle \boldsymbol{p} \times \boldsymbol{E} \rangle \tag{5}$$

acts on the particle. If a linearly polarized electric field of amplitude E, aligned with the x-axis, acts on an elongated particle that is oriented with its long axis in the xy plane, forming an angle β with the x-axis (and the electric field), the torque on the particle is

$$\tau = \hat{z}\frac{n_m^2}{4} Re[\alpha_{\parallel} - \alpha_{\perp}] \sin 2\beta |\boldsymbol{E}|^2 \tag{6}$$

which tends to align the particle orientation with the field (for sufficiently low photon energies). Here $\hat{z}$ is the z unit vector and $\alpha_{\parallel}$ and $\alpha_{\perp}$ are the polarizabilities parallel and perpendicular to the long axis of the particle, respectively. However, eq 5 also encompasses other situations. For example, for a circularly polarized field of angular frequency ω, $\boldsymbol{E} = E(\hat{x} \cos \omega t + \hat{y} \sin \omega t)/\sqrt{2}$, incident on an isotropic particle with polarizability α, we get

$$\tau = \hat{z}\frac{n_m^2}{2} \mathrm{Im}[\alpha] |E|^2 \tag{7}$$

which corresponds to an angular momentum equal to $\hbar$ being transferred to the particle, setting it into rotational motion around the z-axis, for each photon absorbed (as Im[α] describes the absorption by the particle). As will be discussed below, the optical torque opens the possibility of controlling nanoparticle orientation and rotation. On one hand, a slow change of the field direction can be used to manipulate the orientation of a particle, in accordance with eq 6. On the other hand, the intrinsic angular momentum carried by circularly polarized light can also be used to set a nanoparticle into rotation as a consequence of eq 7.

Interparticle Forces. When studying colloidal solutions using laser tweezers, it is not unusual to find that several particles get caught in the optical trap by accident, in particular, when the colloid density is high. Though this is often a problem, it also leaves room for interesting studies of forces and interactions between particles in solution. There have so far only been a few experimental studies concerning metal colloids,[24,44,46] but several theoretical investigations of such effects have been reported in the literature.[37,41,47−57] For example, Li *et al.*[49] studied the optical forces between two spherical metal particles, one caught in a Gaussian laser trap and the other stuck on a surface, and found that both attractive and repulsive interactions could occur depending on the particles' plasmon resonances, the illumination wavelength, and the distance between the laser focus and the position of the immobilized particle. Similarly, Nome *et al.*[24] reported that the optical forces within gold bipyramidal nanoparticle dimers change from attractive to repulsive, depending on the dimer configuration being side-by-side, head-to-tail, or face-on, while Miljković *et al.*[41] discussed under which circumstances optical forces can result in a stable equilibrium distance between two particles. The latter report also points out that the method for calculating interparticle forces has to be chosen with care and that simplified force models may lead to serious errors, in particular, in the case of strongly interacting particles.[41] In general, in eq 1, the effects of all contributions to the electromagnetic field, incident as well as scattered, should be used to calculate the forces on each of the particles in an assembly. However, as in the single-particle case, much can be learned from viewing the mutual forces as the result of electric dipoles either attracting or repelling each other.

For large interparticle distances, where the induced dipolar far-fields dominate, optical binding may occur. The particles will then tend to localize in potential wells created by the interference of the incident electromagnetic field and the light scattered by the surrounding particles.[58,59] At shorter particle−particle distances, the optical force can be either attractive or repulsive depending on how the particles are arranged relative to the directions of light propagation and light polarization. Figure 4 shows in a schematic way how the particles in a heterodimer interact. With an incident field aligned with the dimer axis at low frequencies, one gets two dipoles lined up attracting each other (opposite charges are induced on the different particles near each other). Once the frequency is increased beyond the resonance of the larger particle and below that of the smaller one, its response will lag behind the external field, now producing two dipoles out of phase with each other that instead repel each other. For even higher frequencies than the resonance of the smaller particle, both dipoles will lag behind the field and again attract each other. On the other hand, for an incident field that is perpendicular to the dimer axis (bottom row of the figure), the resulting orientation of the dipoles instead leads to the opposite sequence of forces, repulsive−attractive−repulsive.

EXPERIMENTAL STUDIES

Trapping of Metal Colloids in 3D by Focused Gaussian Beams. A single Gaussian laser beam focused by a microscope objective constitutes the classical laser tweezer setup and provides by far the simplest and most common means for optical trapping and manipulation of a large

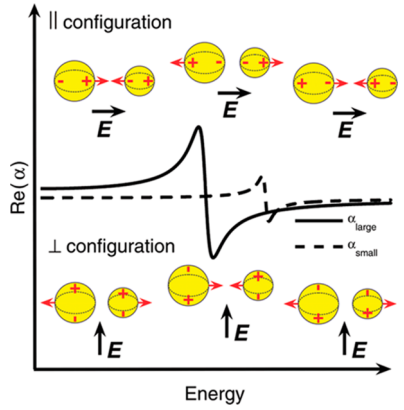

Figure 4. Schematic illustration of the optical forces between two spherical particles in a heterodimer based on a simplified dipole−dipole coupling analysis. The solid and dashed lines indicate the real part of the particle polarizability *versus* photon energy for the large and the small particle, respectively. The interaction can be either attractive or repulsive depending on whether the incident polarization is parallel or perpendicular to the dimer axis and depending on whether the photon energy is higher, lower, or between the two plasmon resonance energies. Reprinted from ref 41. Copyright 2010 American Chemical Society.

variety of objects. Trapping of metal particles in 3D requires a particularly deep optical potential well that can compensate for plasmon-enhanced radiation pressure and increased Brownian motion due to particle heating.[46] It then becomes crucial to minimize optical aberrations in order to achieve a well-defined focal spot and to maximize gradient forces by using high NA immersion optics.

Spherical aberration is the most serious objective aberration when it comes to focusing of monochromatic beams and can in some cases even cause off-axis particle localization in the optical trap.[60] However, Gaussian beams can be made nearly aberration free by adjusting the tube length of the microscope such that the effect of the refractive index mismatch between the immersion medium and the specimen is compensated for.[61] Hajizadeh *et al.* investigated trapping of gold colloids in water using an oil immersion objective and showed that this aberration correction technique allows for stable 3D trapping of particles with diameters down to 9.5 nm, the smallest reported to date.[62] The first demonstration of trapping of silver nanoparticles in 3D was also achieved using oil immersion optics: by optimizing the refractive index of the immersion oil and by choosing an appropriate focal depth, particles with diameters ranging from 20 to 275 nm could be successfully trapped.[63,64] Spherical aberrations are also effectively suppressed by using water immersion objectives, as demonstrated in ref 22, where gold nanoparticles with diameters down to 18 nm were trapped in 3D. The same report also showed that a slight overfilling of the objective's back-aperture by the laser beam dramatically improved the trapping efficiency. An interesting complementary approach to improve trapping stability is to compensate the Brownian motion of the trapped particle using active feedback control of the laser power in response to the particle's position in the trap.[65,66] Balijepalli *et al.* showed that this technique could increase the residence time of a 100 nm gold particle in the trap by up to 26 times.[65]

Quantifying Trap Strengths. As discussed above, a subwavelength particle trapped in a focused laser field experiences a restoring gradient force that can be described in terms of a parabolic optical potential well to a first approximation. The rule of thumb for stable 3D trapping is that the potential depth should be on the order 10 k_BT or more.[67] The strength of the particle's confinement to the trap is usually characterized through the trap stiffness κ, corresponding to the spring constant in Hooke's law. The trap stiffness can, for example, be determined by a measurement of the thermal position fluctuations $x(t)$ of the particle according to

$$\kappa = 2\pi f_0 \gamma \tag{8}$$

where f_0 is the roll-off frequency of the power spectrum of $x(t)$ and γ is the viscous drag coefficient, which can be estimated from the particle geometry and the viscosity of the medium. For a Gaussian trapping beam, the forces are typically on the order of piconewtons for milliwatt laser powers. The position fluctuations can also be used for a more precise determination of the shape of the optical potential well;[62] see ref 68 for a computational toolbox for optical tweezers.

As already stated, the enhanced polarizability of metallic particles compared to dielectric particles of the same size can lead to stronger optical forces and therefore an enhanced trap stiffness. This was first demonstrated by Svoboda and Block[8] for R = 18 nm gold nanoparticles and subsequently in ref 69 by comparing R = 50 nm gold particles to polystyrene beads of the same size. Both studies suggested about 6−7-fold enhancement, depending on how the stiffness was determined. There have been several studies of how the trapping properties of metal nanoparticles depend on particle size.[22,62,70] Figure 5 gives an example of trap stiffness *versus* particle radius for a 1064 nm 3D laser tweezer.[22] The point dipole approximation indicates that the trapping strength is proportional to R^3, reflecting the volume dependence of the dipole polarizability, but for particles with radii larger than the skin depth (which is about 23 nm for gold at the trapping wavelength 1064 nm[22]), one may expect a weaker R^2 dependence due to the partial polarization of the particle. However, the trap strength increases more slowly than expected, as can be seen from Figure 5. This was explained as a result of an increasing scattering component of the radiation pressure, which results in larger particles being pushed further from the focus, thus leading to smaller trap stiffness in both axial

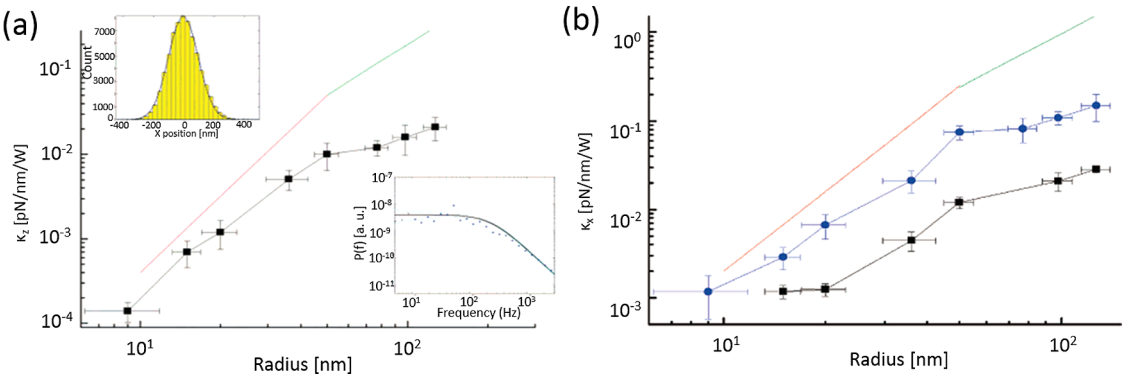

Figure 5. Trap stiffness normalized to trapping laser power *versus* gold particle radius, *R*, in directions parallel (a) and perpendicular (b) to the laser propagation direction. The red and green lines indicate R^3 and R^2 dependencies, respectively. The top and bottom insets in (a) represent the position distribution of the particle and the power spectrum for a *R* = 35 nm particle, respectively. The blue circles and black squares in (b) correspond to measurements with water and oil immersion objectives, respectively, demonstrating the superior spherical aberration corrections in the former case. Reproduced from ref 22. Copyright 2005 American Chemical Society.

and transverse directions.[22] The trap stiffness experienced by nanorods is not expected to scale simply with volume even for small particles since the polarizability is anisotropic and also depends on the aspect ratio of the rod.[71]

Alignement and Rotation of Plasmonic Nanostructures. As outlined in the theory section, anisotropic particles tend to align in a linearly polarized trap such that the total potential energy is minimized. For an elongated particle, this typically implies that the long axis of the particle will point along the polarization vector.[25,35,71] The same effect occurs for a particle dimer, for which the polarizability tensor has the same symmetry as that of a nanorod/elongated nanoparticle.[44] Metal nanowires, on the other hand, have been shown to align perpendicularly to the polarization, indicating that the polarizability component perpendicular to the wire is larger than the parallel component in this case (cf. eq 6).[25,72] Nanorods have been predicted to align perpendicularly to the polarization when the trapping wavelength is shorter than the longitudinal plasmon resonance for the same reason.[73]

Ruijgrok *et al.*[74] estimated the torque experienced by gold nanorods with a length of 100 nm and an aspect ratio of ≈2.4 trapped in 3D using linear polarized laser tweezers (λ = 1064 nm, *P* = 80 mW) to ∼100 pN·nm. The measurement was based on the time-averaged distribution of the nanorod orientation deduced from white-light scattering spectra and an autocorrelation analysis of rotational Brownian fluctuations observed in the polarized scattered intensity. The tendency to align has also been verified by measurements of two-photon fluorescence emitted by freely diffusing nanorods, as shown in Figure 6a.[35] The intensity autocorrelation function exhibits a distinct shoulder at short times due to free rotational diffusion, but this component decreases in amplitude when the intensity of the linearly polarized laser beam (λ = 850 nm) is increased, signaling alignment along the polarization direction (dotted curves). The alignment effect has also been verified directly by monitoring dark-field scattering spectra of nanorods trapped in 2D, as shown in Figure 6b.[25] The intensity of the longitudinal LSP peak is maximized when the laser (λ = 830 nm) polarization is parallel to the white light excitation polarization and vanishes if the polarizations are perpendicular. The perpendicular alignment of a silver nanowire to the laser (λ = 830 nm) polarization is shown in Figure 6c. From panel I to III, it is clear that the nanowire follows the linear polarization of the trapping laser as it is turning. It is also possible to use the alignment effect to spin the wire by rotating the polarization at high speed. The direction of the wire will then tend to lag behind the polarization direction due to the viscous drag force, and the nanowire will tend to slip if the polarization rotation is fast enough.[25] The lag in rotation has been suggested as a probe of the viscosity of the immersion medium.[75]

Direct transfer of torque from circularly polarized light (cf. eq 7) obviously provides a much more convenient method to spin particles than mechanical rotation of a polarizer. The particle rotation is in this case a direct consequence of conservation of photon spin angular momentum (SAM); whereas dielectric non-absorbing particles need to be birefringent for this to occur, SAM transfer to metal colloids is dominated by absorption.[25,45,76,77] Figure 7a illustrates that this method can be used to spin large gold colloids (average radius ∼200 nm) about their own axes with frequencies on the order of 3 kHz or more, the highest reported to date for particles in water.[45] The particles were trapped in 2D, using a λ = 830 nm laser beam with a power of ∼10−50 mW at the sample, and the spinning was revealed by measuring the intensity autocorrelation of light scattered from the trapped particle: the correlation function exhibits a periodic oscillation when the particle spins due to SAM transfer from circularly polarized light, whereas it decays

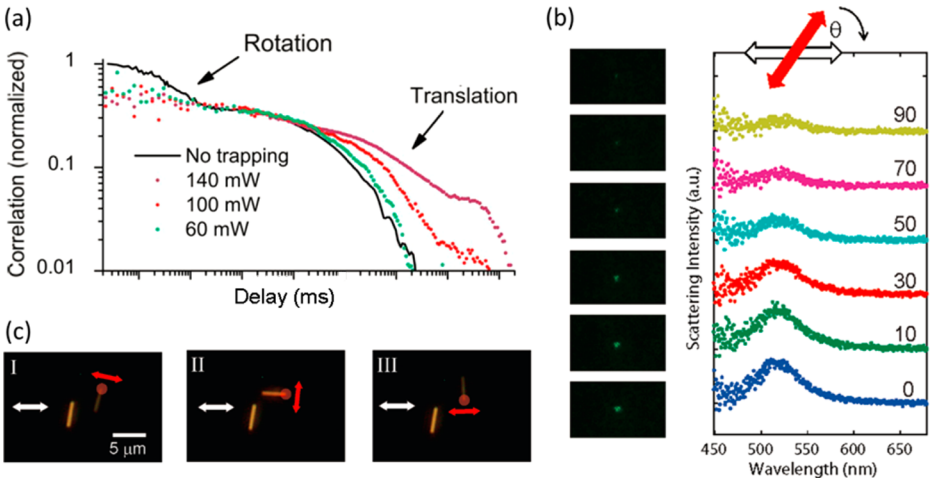

Figure 6. (a) Alignment of gold nanorods in the presence of a linearly polarized laser field is revealed by the decrease in the rotational diffusion component of the two-photon luminescence intensity autocorrelation signal of the nanorod. Reprinted with permission from ref 35. Copyright 2006 Optical Society of America. (b) Scattering spectra measured using polarized white light (white arrow) *versus* trapping laser polarization (red arrow) show that silver nanorods align parallel to the electric field orientation of the trapping light. (c) Silver nanowires instead align perpendicular to the laser polarization (red arrow) and can be rotated by turning the laser polarization. Reprinted from ref 25. Copyright 2010 American Chemical Society.

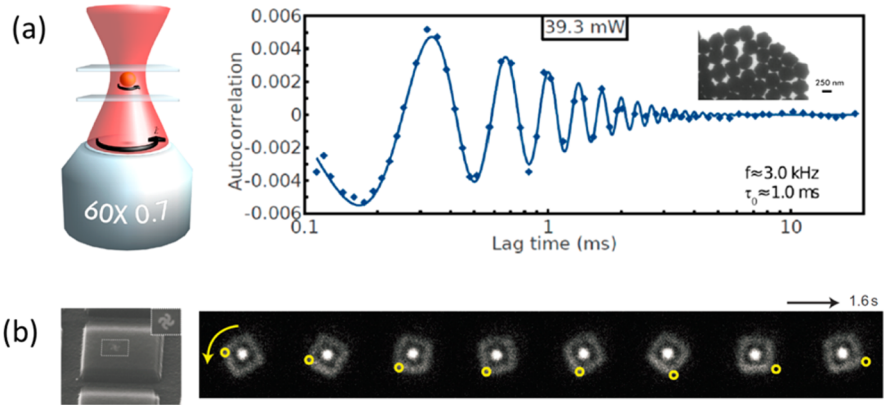

Figure 7. (a) Spinning of a trapped gold nanoparticle using a circularly polarized laser beam. Reproduced from ref 45. Copyright 2013 American Chemical Society. (b) Gammadion-shaped gold nanostructure (left panel) was used as a nanoscale plasmonic motor to rotate a microdisk that was ~4000 times larger than the gammadion itself (right panel). Reproduced with permission from ref 81. Copyright 2010 Macmillan Publishers Ltd.

monotonously for linearly polarized light. Comparisons with theory indicated that the high spinning frequencies observed experimentally were partly due to particle heating and a corresponding decrease of the viscous torque by the water surrounding the particles.

If a structure is optically large and at the same time highly asymmetric, it is possible to induce rotation through anisotropic radiation pressure even if the polarization is linear, the so-called optical windmill effect. This was argued to be an important cause of rotation for micron-sized gold nanorods and nanoparticle aggregates.[78−80] It is possible that the windmill effect is also the main mechanism behind the rotation of lithographically prepared gammadion-shaped plasmonic particles reported in ref 81. These structures were used to rotate dielectric microdisks 4000 times larger than the particle itself, albeit with rather low rotation frequencies of the order of hertz (Figure 7b).

Trapping and Manipulation of Metal Colloids Using Unconventional Laser Fields. Higher order Laguerre−Gaussian (LG) laser modes provide many possibilities for trapping and manipulation experiments that are impossible using conventional laser tweezers. An LG mode constitutes an optical vortex with an annular intensity distribution and incorporates an azimuthal phase structure of $e^{il\varphi}$, where φ is the azimuthal angle and l is an integer describing the mode index (also known as the charge or quantum number of the mode).[82] The intensity distributions corresponding to different LG modes are shown in Figure 8a. Whether a particle will be trapped into the bright rings or confined to the dark regions depends on the sign of the particle polarizability, which determines whether the gradient

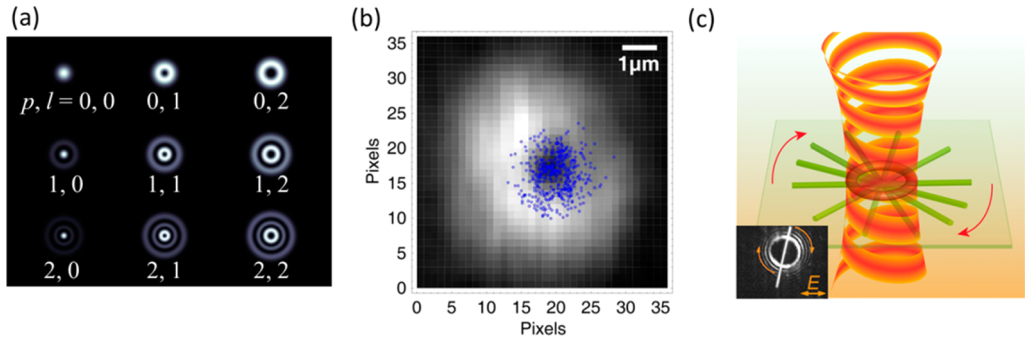

Figure 8. (a) Simulated intensity distribution of different Laguerre–Gaussian (LG) modes with *p* and *l* being the radial index and the charge number, respectively. (b) Spatial data points for the movement of a gold nanoparticle confined to a LG beam with charge index *l* = 2 with blue-detuned laser wavelength with respect to the LSP. The particle preferentially resides in the dark region of the beam. Reprinted with permission from ref 83. Copyright 2008 Optical Society of America. (c) Illustration of the rotation of a silver nanowire by the orbital angular momentum of a LG beam. The dark-field image is shown in the inset. Reprinted from ref 90. Copyright 2013 American Chemical Society.

forces are repulsive or attractive, and on the relative magnitudes of the scattering and gradient forces.[83,84] An interesting example of trapping with an annular field was given by Dienerowitz *et al.*[83] Gold nanoparticles with diameters of 100 and 250 nm were trapped by using a laser wavelength on the blue side of the LSP, that is, where gradient forces are expected to be repulsive due to the sign change of the polarizability. The particles were indeed confined into the dark core of the beam, as illustrated in Figure 8b. This methodology is interesting because it may provide a means for manipulation of plasmonic particles with negligible laser absorption and heating. Another example of trapping with an annular beam was given in ref 85, in which a silver nanowire was trapped in 3D by using a so-called Fourier-transformed Bessel beam, which has an extended focus depth, in combination with its back-reflection from a mirror to compensate for the radiation pressure. It has also been argued that radially polarized beams with an annular intensity distribution could facilitate 3D trapping of metal particles.[86] However, this claim was recently disputed based on the omission of the aforementioned curl force in the calculation.[87] Further theoretical and experimental investigations of how different force components contribute in annular beams are clearly wanted.[88,89]

An important property of a LG beam is that it carries orbital angular momentum (OAM) of $l\hbar$ per photon that can be transferred to a trapped particle by absorption and scattering. OAM is distinct from the SAM of circularly polarized light, but it can also set particles into rotational motion. The particles will rotate around their own axis if they are significantly larger than the diameter of the annular intensity distribution of the LG beam.[77,90,91] Figure 8c shows an example of this effect from a study by Yan *et al.*[90] on ~10 μm long silver nanowires. Smaller particles will instead rotate in an orbit around the optical axis.[83,92]

Colloidal metal particles can also be trapped using pulsed laser fields. Jiang *et al.*[93] used 100 fs near-infrared pulses in a standard single-beam optical tweezers setup to trap gold particles (R = 30 nm) in 2D. For high laser powers, it was found that a single particle could jump between two equivalent sites aligned along the linear laser polarization. The phenomenon was interpreted in terms of a nonlinear-induced polarization of the nanoparticle, which resulted in a split of the optical potential well.

We should finally note that it is also possible to trap metal nanoparticles using evanescent near-fields, for example, produced by dielectric or plasmonic waveguides[94–97] or in the gaps in plasmonic dimer nanoantennas.[98,99] However, the particles will then be confined to the surface of the structure, where the near-fields are strongest. An interesting development of this approach was recently reported by Berthelot *et al.*,[100] who used a dimer antenna attached to the end of an optical fiber for 3D optical manipulation of small dielectric particles in solution.

Dimerization and Aggregation of Metal Colloids Using Optical Forces. As outlined before, the optical interaction between nanoparticles subject to intense laser illumination can lead to both attractive and repulsive interparticle forces. If a spatially extended laser field illuminates particles that are free to move in one or two dimensions, the particles tend to organize in a lattice with a lattice constant given by the illumination wavelength.[58,59] This kind of "optical binding" phenomenon is due to interference between the far-field components of the dipolar fields scattered by the particles and therefore highly sensitive to the particles scattering efficiency. Demergis and Florian took advantage of the high scattering cross section of large gold particles (R = 100 nm) in a study of optical binding in water using a standing wave optical line trap.[101] The particles could be organized in pairs with well-defined interparticle separation given by multiples of the trapping wavelength in water (λ = 1064/1.33 nm), and smaller particles (R = 50 nm) could be stably trapped between the larger particles. The authors concluded that the interparticle optical forces could be more than

20 times stronger than the gradient forces exerted by the line trap.

If several colloidal metal particles are instead trapped by a focused laser beam, the near-field components of the optical interparticle force will dominate. This typically results in particles forming dense lines directed along the incident polarization direction, although other particle arrangements are, in principle, also possible depending on the relation between the incident wavelength and the particle plasmon resonances.[41] The average interparticle distances will depend on the strength of the optical interaction, the thermal movement of the particles, as well as on the colloid interaction "in the dark", as specified by the Coulomb repulsion between the particles surface charges and the van der Waals attraction.[102]

The techniques available for single-particle optical force measurements are not easily adapted to studies of interacting particles. Indirect experimental evidence for near-field interparticle forces primarily comes from measurements of changes in spectroscopic properties.[24,42−44,46,103,104] Two spherical metal nanoparticles that are coupled into a pair due to the near-field optical forces will exhibit a scattering spectrum similar to a single nanorod. In particular, the pair will exhibit a plasmon mode that is red-shifted compared to the single-particle plasmon, and the degree of red shift will sensitively depend on the interparticle separation.[105,106] Tong *et al.*[44] utilized this "plasmon ruler" methodology to probe the interaction within pairs of colloidal gold particles (R = 40 nm) trapped in 2D by a single focused laser beam (λ_0 = 830 nm). The electrostatic repulsion between the particles could be controlled through screening of the surface charges by adding different amounts of salt to the colloid solution. As shown in Figure 9, increasing salt concentration led to a split of the plasmon band and a progressively stronger red shift of the plasmon polarized parallel to the dimer axis, signaling a decreased particle separation. A comparison between the experimental red shift and theory indicated that the equilibrium surface separation was ∼9 nm for the highest salt concentration (20 mM), and that the corresponding depth of the potential well was on the order ∼5 k_BT. The pair formation was shown to be reversible for salt concentrations up to 20 mM; that is, the pair broke up and the particles escaped into solution if the laser was blocked, while higher salt contents led to irreversible aggregation.

There have been a number of reports on trapping laser illumination resulting in particle aggregation.[57,107−111] Formation of larger particle aggregates in a trap leads to a plasmon red shift that tends to increase with the number of particles in the aggregate. If the trapping laser wavelength is to the red of the single-particle resonance wavelength, which is usually the case, aggregation may cause the collective

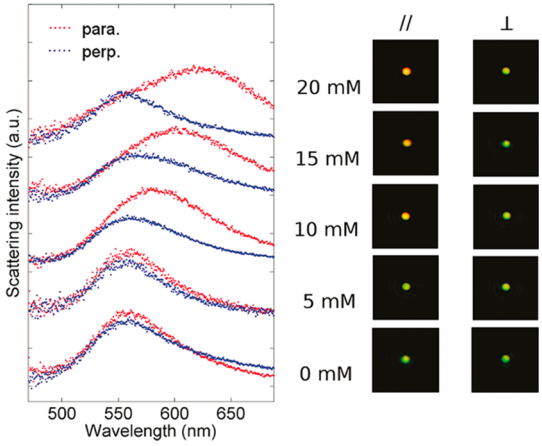

Figure 9. Elastic scattering spectra (left) and images (right) of optically trapped gold particle pairs *versus* salt concentration. The incident white light polarization was either parallel (red) or perpendicular (blue) to the laser tweezers' polarization (∼2 mW/μm^2, λ_0 = 830 nm). The polarization dependence shows that the particle pair orients itself parallel to the laser polarization, and the increasing red shift shows that that the particle separation decreases for higher salt concentrations. Reprinted from ref 44. Copyright 2011 American Chemical Society.

plasmon resonance to overlap with the laser wavelength. This results in stronger gradient and interparticle optical forces but also increased absorption. Ohlinger *et al.* found that the trapping stability of silver particle aggregates increased with the number of particles up to the point of spectral overlap, after which particles were thermally ejected from the aggregate.[46] However, it is possible that other factors apart from optical and thermal forces also play a role in the laser-induced aggregation effect. For example, Zhang *et al.*[112] found that experimentally observed aggregates were larger than the spot size of the Gaussian trapping beam and argued that the laser-induced heating could liberate capping ions from the surface of the particles, thus reducing electrostatic repulsion and promoting aggregation.

As mentioned above, nanoparticles tend to form linear assemblies aligned along the trapping laser polarization.[70,108,109,113] Iida *et al.*[113] simulated particle aggregation in an linearly polarized optical trap, taking into account both optical and colloidal interactions. Figure 10 shows the resulting particle positions obtained for the cases when two or eight R = 20 nm gold particles are released close to the near-IR laser focus (λ_0 = 1064 nm). The figure shows that a dimer aligned parallel to the laser polarization is formed in the trap in the first case (Figure 10a), in agreement with the experimental data shown in Figure 9, while an elongated aggregate is formed in the second case (Figure 10b) due to the interplay between the short-range interparticle forces and the gradient force caused by the confinement of the laser field.

Surface-Enhanced Raman Spectroscopy of Optically Trapped Metal Colloids. The nanometric gaps and crevices that

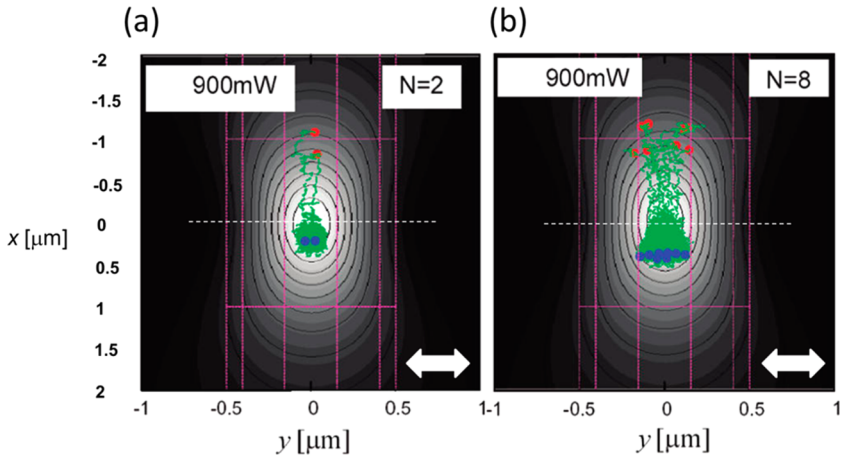

Figure 10. Simulation of Brownian motion and laser-induced aggregation of gold nanoparticles. The red and blue dots indicate the initial and final positions of the particles, respectively. The white arrows indicate the laser polarization direction, and the horizontal dashed white line indicates the focal plane. The trajectories of the particles are represented by the green curves. Reproduced from ref 113. Copyright 2012 American Chemical Society.

result from optical aggregation of plasmonic nanoparticles lead to large field enhancement and "hot spots" suitable for optical-tweezers-based surface-enhanced Raman scattering molecular spectroscopy.[107,109,114,115] Svedberg *et al.* reported on SERS from optically trapped silver nanoparticles ($R \approx 40$ nm) functionalized by a layer of thiophenol molecules, which acts as a SERS probe and lowers the electrostatic repulsion between particles to enable aggregation.[43] Single silver particles were optically manipulated to pair up with immobilized particles, which resulted in an increase of the SERS signal by a factor of 20 or more.[43] The strong optical near-fields present in the gap regions may also amplify SERS by actively pulling molecules into the gaps through enhanced gradient forces.[57] Tanaka *et al.* investigated SERS and Rayleigh scattering from silver nanoparticles ($R \approx 15$ nm) trapped into globular and linear aggregates using circularly and linearly polarized laser light, respectively.[109] It was found that pseudoisocyanine could be detected down to a concentration of 10^{-14} M in the linear aggregates, and the authors argued that this result demonstrated that the molecules were selectively adsorbed to the corresponding gap hot spots by optical forces.

The combination of optical manipulation, optical aggregation, and SERS is also interesting for lab-on-a-chip-based molecular sensing.[107,116] An example is shown in Figure 11.[107] Optical aggregation was induced by a $\lambda_0 = 830$ nm trapping beam focused at the confluence of two microfluidic channels, one carrying silver colloids and the other carrying a molecular solution (Figure 11a). As a nanoparticle aggregate grows with time, as indicated by the dark-field images (Figure 11b), so does the intensity of SERS from thiolphenol molecules adsorbed on the particles (Figure 11c). Similarly, Lin *et al.* demonstrated successful SERS sensing based on colloid trapping in a photonic

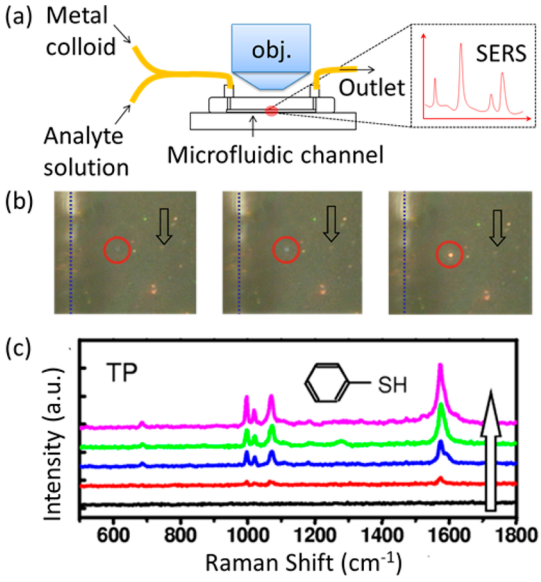

Figure 11. Optical tweezing and SERS in a microfluidics device. (a) Schematic of the experimental setup. (b) Dark-field images showing gradual optical aggregation of trapped silver nanoparticles at the confluence of the colloid and analyte flow channels. The vertical dashed lines and the arrows indicate the edge of the microfluidic channel and the direction of the flow, respectively. (c) Time sequence of thiophenol SERS spectra measured on the optically induced aggregate. Reproduced with permission from ref 107. Copyright 2009 The Royal Society of Chemistry.

crystal cavity integrated in a microfluidic device.[116] The advantage of these approaches to SERS sensing is that it is easy to switch between different analyte solutions, that the SERS substrate can be continuously renewed through the colloid flow, and that the material consumption is extremely small.

Surface Immobilization and Sorting of Plasmonic Nanoparticles Using Optical Forces. Optical manipulation can be used to build complex surface-bound plasmonic nanostructures with high precision.[117−121] The basic idea is

to move a metal colloid particle close enough to a substrate, for example, by using the radiation pressure force, where the attractive force between the substrate and the particle dominates so that the particle will get stuck. Some of the main advantages of the methodology, compared to standard nanofabrication, are that colloidal nanoparticles typically have much higher crystal quality than particles made by lithographic methods and that particles can be deposited in very confined spaces, such as inside microfluidic devices. The positional accuracy of the method will sensitively depend on the balance between lateral gradient forces, Brownian particle motion, and radiation pressure, which in turn depends on particle properties, laser power, and laser wavelength. Urban *et al.*[119] demonstrated that single spherical gold particles (R = 40 nm) could be "printed" with a precision of ~50 nm, that is, significantly better than the optical diffraction limit, using a laser wavelength close to the particle resonance (λ_0 = 532 nm). The particles were coated with a polyelectrolyte to create a positive surface charge in order to avoid spontaneous adsorption onto the substrate, and it was shown that an increase in laser power decreased the positioning accuracy due to the enhanced Brownian motion. Guffey and Scherer[117] showed that areas up to tens of square micrometers in size could be patterned with gold particles, while Nedev *et al.*[118] utilized multiple beams created by a spatial light modulator to imprint several particles simultaneously onto a substrate. Recent developments include the use of optical torques to align nanorods before surface attachment[121] and the use of optical aggregation to build large arrays of nanoparticles.[120]

Since the optical forces on metallic particles vary dramatically with particle shape, size, and composition, in particular, near resonance, interesting opportunities for size/shape-selective optical sorting emerge.[122−124] Ploschner *et al.*[122] used size-dependent differences in radiation pressure to separate out larger from smaller gold particles in a colloid solution. The method was based on using a total internal reflection objective to launch two overlapping but counter-propagating evanescent waves at different wavelengths (532 and 671 nm) close to the plasmon resonances of the particles. A related methodology was recently used to separate out and selectively deposit bipyramidal gold nanoparticles based on plasmon-enhanced radiation pressure effects.[124]

Heating of Optically Trapped Metal Colloids. The particle heating associated with optical trapping of metal colloids is usually considered detrimental for practical applications. However, several studies have shown that heating can be controlled and in some cases even taken advantage of.[125−130] For example, Feldmann and co-workers recently showed controlled hybridization of DNA connecting pairs of gold particles trapped off resonance,[128] and the same group demonstrated

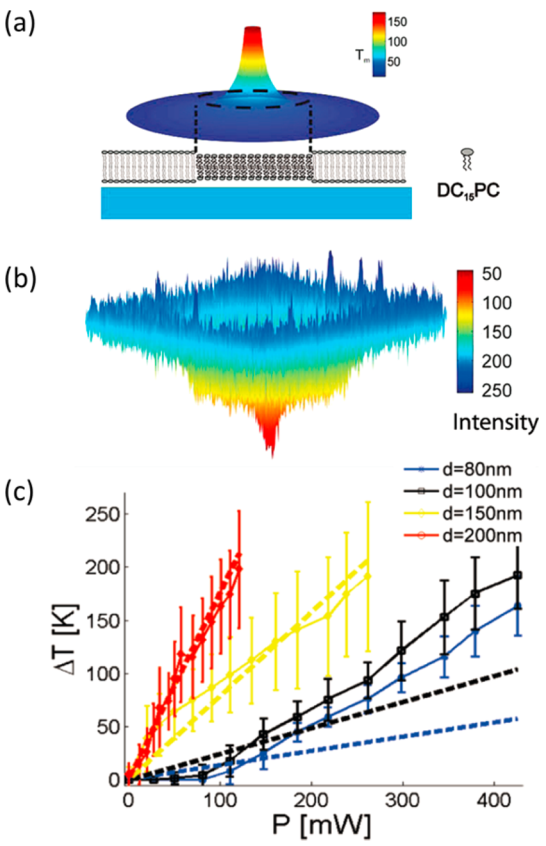

Figure 12. Estimating particle surface temperatures using a lipid bilayer phase transition. (a) Optically trapped and laser-heated gold nanoparticle above a lipid bilayer that has melted in a region with a temperature above 33 °C, indicated by T_m. (b) Fluorescence intensity measured at the vicinity of the trapped gold nanoparticle. (c) Estimated surface temperature increase *versus* applied laser power for different particle diameters *d*. The wavelength of the trapping laser was 1064 nm. The dashed lines indicate theoretical estimates. Reprinted from ref 125. Copyright 2010 American Chemical Society.

that optical manipulation of laser-heated gold particles can be used for enhanced photochemistry[129] and nanolithography of polymers based on curing or milling processes.[131,132]

Temperature measurements at the nanoscale are experimentally challenging. Nevertheless, a few attempts to quantify laser-induced heating of optically trapped metal colloids have been reported.[125,126] Bendix *et al.*[125] used supported lipid bilayers loaded with fluorescent molecules to probe the heat generated by gold particles trapped in 2D by a 1064 nm laser tweezer (see Figure 12). The bilayer exhibits a gel-to-liquid phase transition at 33 °C that results in the decreased fluorescence intensity. With the temperature of the sample chamber set to 28 °C, a dark melted area with a temperature exceeding 33 °C appeared around a trapped particle for sufficiently high laser powers (Figure 12a,b). The size of this area could be used to estimate the corresponding temperature increase at the particle surface for different particle radii, as shown in Figure 12c. The authors found that the

temperature increase scaled linearly with the applied laser power but with heating rates increasing rapidly with particle size, reflecting the increased absorption cross section at near-infrared wavelengths (see Figure 3a). A subsequent study of heating of 3D trapped Au particles based on a similar methodology obtained analogous results for particles with diameters up to 100 nm.[126] However, larger particles exhibited reduced heating, probably because the radiation pressure forced these particles away from the laser focus. It should be pointed out that neither of these studies[103,104] nor the previously mentioned studies of particle rotation[89] and enhanced surface chemistry[107] found evidence for water vapor bubble formation despite estimated particle surface temperatures far above 100 °C. However, a very recent paper by Li *et al.* reported bubble formation around single trapped nanoparticles during the optical injection into cells.[133]

OUTLOOK

Twenty years have passed since the first experimental study of metal colloids using optical tweezers.[8] Although the number of published reports has increased steadily, the field is still relatively unexplored compared to many other areas of nano-optics. Hence, there is plenty of room for further developments.

As should be clear from this review, the vast majority of reported optical tweezing studies of metal colloids deal with silver and, in particular, gold particles. Although this is well-motivated from the point of view of plasmonics and biophysics, there is no doubt about many interesting avenues for exploring and utilizing optical forces on metal colloids composed of or containing other materials, for example, with catalytic, magnetic, or light-harvesting properties. Likewise, only a few of the vast number of currently available colloid shapes, which range from relatively simple structures like cubes and core−shell particles to complex geometries like nanostars, have been investigated using optical tweezers methodologies.

Our ability to predict optical forces, plasmonic properties, and laser heating effects has improved tremendously over the past few years due to the development of a number of sophisticated software solutions for electromagnetics simulations. However, accurate calculations for cases that involve nontrivial particle shapes and laser fields remain a challenge. Continued developments in computational electromagnetics will likely improve this situation and may give possibilities for detailed *in silico* experiments and optimization algorithms, along with developing further qualitative understanding and easy-to-use approximations for optical forces.

Optical aggregation of Ag colloids has proven to be highly efficient for generating SERS, but there are a number of other molecular spectroscopies, including surface-enhanced infrared absorption, surface-enhanced fluorescence, and various nonlinear processes, for which the advantages offered by optical manipulation remain untested. Biomolecular analysis based on refractive index changes near metal surfaces, so-called surface plasmon resonance sensing, is a key application of plasmonics but completely unexplored in the context of optical tweezing of plasmonic nanoparticles.

Laser-induced heating of optically tweezed metal colloids remains an Achilles heel for many applications, in particular, in the life science area, but, as demonstrated by several recent reports, also gives unique possibilities for extremely localized delivery of thermal energy. Both the molecular spectroscopy and laser heating opportunities are probably best taken advantage of in combination with applications that require confined spaces or have limited physical access, such as in bioassays based on microfluidics or in single-cell experiments.[130,133]

Last but not least, laser tweezing of metal colloids offers immense opportunities for curiosity-driven research in diverse areas of high current interest, including photonic forces, in general, nano-optical and colloid interactions, vapor formation and other phase transitions, light-driven nanomachines, and other opto-mechanical applications, nanoscale rheology, and much more. It is simply great fun!

Conflict of Interest: The authors declare no competing financial interest.

Acknowledgment. This work was supported by the Knut and Alice Wallenberg Foundation, the Emil Aaltonen Foundation, the National Natural Science Foundation of China (Grant No. 11374355), and the Ministry of Science and Technology of China (Grant No. 2012YQ12006005). We thank Faegheh Hajizadeh and Shao Lei for comments on the manuscript, and Michael Taylor for help with graphics.

REFERENCES AND NOTES

1. Ashkin, A. Acceleration and Trapping of Particles by Radiation Pressure. *Phys. Rev. Lett.* **1970**, *24*, 156–159.
2. Ashkin, A.; Dziedzic, J. M.; Bjorkholm, J. E.; Chu, S. Observation of a Single-Beam Gradient Force Optical Trap for Dielectric Particles. *Opt. Lett.* **1986**, *11*, 288–290.
3. Phillips, W. D. Laser Cooling and Trapping of Neutral Atoms. *Rev. Mod. Phys.* **1998**, *70*, 721–741.
4. Dholakia, K.; Reece, P.; Gu, M. Optical Micromanipulation. *Chem. Soc. Rev.* **2008**, *37*, 42–55.
5. Dienerowitz, M.; Mazilu, M.; Dholakia, K. Optical Manipulation of Nanoparticles: A Review. *J. Nanophotonics* **2008**, *2*, 021875.
6. Ashok, P. C.; Dholakia, K. Optical Trapping for Analytical Biotechnology. *Curr. Opin. Biotechnol.* **2012**, *23*, 16–21.
7. Fazal, F. M.; Block, S. M. Optical Tweezers Study Life under Tension. *Nat. Photonics* **2011**, *5*, 318–321.
8. Svoboda, K.; Block, S. M. Optical Trapping of Metallic Rayleigh Particles. *Opt. Lett.* **1994**, *19*, 930–932.
9. Hutter, E.; Fendler, J. H. Exploitation of Localized Surface Plasmon Resonance. *Adv. Mater.* **2004**, *16*, 1685–1706.
10. Shegai, T.; Chen, S.; Miljković, V. D.; Zengin, G.; Johansson, P.; Käll, M. A Bimetallic Nanoantenna for Directional Colour Routing. *Nat. Commun.* **2011**, *2*, 481.
11. Curto, A. G.; Volpe, G.; Taminiau, T. H.; Kreuzer, M. P.; Quidant, R.; van Hulst, N. F. Unidirectional Emission of a Quantum Dot Coupled to a Nanoantenna. *Science* **2010**, *329*, 930–933.

12. Novotny, L.; van Hulst, N. Antennas for Light. *Nat. Photonics* **2011**, *5*, 83–90.
13. Atwater, H. A.; Polman, A. Plasmonics for Improved Photovoltaic Devices. *Nat. Mater.* **2010**, *9*, 205–213.
14. Neumann, O.; Urban, A. S.; Day, J.; Lal, S.; Nordlander, P.; Halas, N. J. Solar Vapor Generation Enabled by Nanoparticles. *ACS Nano* **2013**, *7*, 42–49.
15. Neumann, O.; Feronti, C.; Neumann, A. D.; Dong, A.; Schell, K.; Lu, B.; Kim, E.; Quinn, M.; Thompson, S.; Grady, N.; et al. Compact Solar Autoclave Based on Steam Generation Using Broadband Light-Harvesting Nanoparticles. *Proc. Natl. Acad. Sci. U.S.A.* **2013**, *110*, 11677–11681.
16. Willets, K. A.; Van Duyne, R. P. Localized Surface Plasmon Resonance Spectroscopy and Sensing. *Annu. Rev. Phys. Chem.* **2007**, *58*, 267–297.
17. Brolo, A. G. Plasmonics for Future Biosensors. *Nat. Photonics* **2012**, *6*, 709–713.
18. Liu, N.; Hentschel, M.; Weiss, T.; Alivisatos, A. P.; Giessen, H. Three-Dimensional Plasmon Rulers. *Science* **2011**, *332*, 1407–1410.
19. Huang, X. H.; Jain, P. K.; El-Sayed, I. H.; El-Sayed, M. A. Plasmonic Photothermal Therapy (PPTT) Using Gold Nanoparticles. *Laser Med. Sci.* **2008**, *23*, 217–228.
20. Karker, N.; Dharmalingam, G.; Carpenter, M. A. Thermal Energy Harvesting Plasmonic Based Chemical Sensors. *ACS Nano* **2014**, *8*, 10953–10962.
21. Xia, Y. N.; Xiong, Y. J.; Lim, B.; Skrabalak, S. E. Shape-Controlled Synthesis of Metal Nanocrystals: Simple Chemistry Meets Complex Physics? *Angew. Chem., Int. Ed.* **2009**, *48*, 60–103.
22. Hansen, P. M.; Bhatia, V. K.; Harrit, N.; Oddershede, L. Expanding the Optical Trapping Range of Gold Nanoparticles. *Nano Lett.* **2005**, *5*, 1937–1942.
23. Hester, B. C.; Crawford, A.; Kishore, R. B.; Helmerson, K.; Halas, N. J.; Levin, C. Optical Trapping of Nanoshells. *Proc. SPIE* **2007**, *6644*, B6441–B6441.
24. Nome, R. A.; Guffey, M. J.; Scherer, N. F.; Gray, S. K. Plasmonic Interactions and Optical Forces between Au Bipyramidal Nanoparticle Dimers. *J. Phys. Chem. A* **2009**, *113*, 4408–4415.
25. Tong, L.; Miljković, V. D.; Käll, M. Alignment, Rotation, and Spinning of Single Plasmonic Nanoparticles and Nanowires Using Polarization Dependent Optical Forces. *Nano Lett.* **2010**, *10*, 268–273.
26. Maragò, O. M.; Jones, P. H.; Gucciardi, P. G.; Volpe, G.; Ferrari, A. C. Optical Trapping and Manipulation of Nanostructures. *Nat. Nanotechnol.* **2013**, *8*, 807–819.
27. Bendix, P. M.; Jauffred, L.; Norregaard, K.; Oddershede, L. B. Optical Trapping of Nanoparticles and Quantum Dots. *IEEE J. Sel. Top. Quantum Electron.* **2014**, *20*, 4800112.
28. Urban, A. S.; Carretero-Palacios, S.; Lutich, A. A.; Lohmuller, T.; Feldmann, J.; Jäckel, F. Optical Trapping and Manipulation of Plasmonic Nanoparticles: Fundamentals, Applications, and Perspectives. *Nanoscale* **2014**, *6*, 4458–4474.
29. Juan, M. L.; Righini, M.; Quidant, R. Plasmon Nano-optical Tweezers. *Nat. Photonics* **2011**, *5*, 349–356.
30. Ashkin, A. Forces of a Single-Beam Gradient Laser Trap on a Dielectric Sphere in the Ray Optics Regime. *Biophys. J.* **1992**, *61*, 569–582.
31. Toussaint, K. C.; Liu, M.; Pelton, M.; Pesic, J.; Guffey, M. J.; Guyot-Sionnest, P.; Scherer, N. F. Plasmon Resonance-Based Optical Trapping of Single and Multiple Au Nanoparticles. *Opt. Express* **2007**, *15*, 12017–12029.
32. Arias-González, J. R.; Nieto-Vesperinas, M. Optical Forces on Small Particles: Attractive and Repulsive Nature and Plasmon-Resonance Conditions. *J. Opt. Soc. Am. A* **2003**, *20*, 1201–1209.
33. Agayan, R. R.; Gittes, F.; Kopelman, R.; Schmidt, C. F. Optical Trapping Near Resonance Absorption. *Appl. Opt.* **2002**, *41*, 2318–2327.
34. Huang, L.; Martin, O. J. F. Reversal of the Optical Force in a Plasmonic Trap. *Opt. Lett.* **2008**, *33*, 3001–3003.
35. Pelton, M.; Liu, M.; Kim, H. Y.; Smith, G.; Guyot-Sionnest, P.; Scherer, N. F. Optical Trapping and Alignment of Single Gold Nanorods by Using Plasmon Resonances. *Opt. Lett.* **2006**, *31*, 2075–2077.
36. Albaladejo, S.; Marqués, M. I.; Laroche, M.; Sáenz, J. J. Scattering Forces from the Curl of the Spin Angular Momentum of a Light Field. *Phys. Rev. Lett.* **2009**, *102*, 113602.
37. Wong, V.; Ratner, M. A. Gradient and Nongradient Contributions to Plasmon-Enhanced Optical Forces on Silver Nanoparticles. *Phys. Rev. B* **2006**, *73*, 075416.
38. Novonty, L.; Hecht, B. *Principles of Nano-optics*; Cambridge University Press: Cambridge, 2006; pp 45−88.
39. Waterman, P. C. Symmetry, Unitarity, and Geometry in Electromagnetic Scattering. *Phys. Rev. D* **1971**, *3*, 825.
40. Barton, J. P.; Alexander, D. R.; Schaub, S. A. Theoretical Determination of Net-Radiation Force and Torque for a Spherical-Particle Illuminated by a Focused Laser-Beam. *J. Appl. Phys.* **1989**, *66*, 4594–4602.
41. Miljković, V. D.; Pakizeh, T.; Sepulveda, B.; Johansson, P.; Käll, M. Optical Forces in Plasmonic Nanoparticle Dimers. *J. Phys. Chem. C* **2010**, *114*, 7472–7479.
42. Prikulis, J.; Svedberg, F.; Käll, M.; Enger, J.; Ramser, K.; Goksör, M.; Hanstorp, D. Optical Spectroscopy of Single Trapped Metal Nanoparticles in Solution. *Nano Lett.* **2004**, *4*, 115–118.
43. Svedberg, F.; Li, Z.; Xu, H.; Käll, M. Creating Hot Nanoparticle Pairs for Surface-Enhanced Raman Spectroscopy through Optical Manipulation. *Nano Lett.* **2006**, *6*, 2639–2641.
44. Tong, L.; Miljković, V. D.; Johansson, P.; Käll, M. Plasmon Hybridization Reveals the Interaction between Individual Colloidal Gold Nanoparticles Confined in an Optical Potential Well. *Nano Lett.* **2011**, *11*, 4505–4508.
45. Lehmuskero, A.; Ogier, R.; Gschneidtner, T.; Johansson, P.; Käll, M. Ultrafast Spinning of Gold Nanoparticles in Water Using Circularly Polarized Light. *Nano Lett.* **2013**, *13*, 3129–3134.
46. Ohlinger, A.; Nedev, S.; Lutich, A. A.; Feldmann, J. Optothermal Escape of Plasmonically Coupled Silver Nanoparticles from a Three-Dimensional Optical Trap. *Nano Lett.* **2011**, *11*, 1770–1774.
47. Hallock, A. J.; Redmond, P. L.; Brus, L. E. Optical Forces between Metallic Particles. *Proc. Natl. Acad. Sci. U.S.A.* **2005**, *102*, 1280–1284.
48. Zelenina, A. S.; Quidant, R.; Nieto-Vesperinas, M. Enhanced Optical Forces between Coupled Resonant Metal Nanoparticles. *Opt. Lett.* **2007**, *32*, 1156–1158.
49. Li, Z.; Käll, M.; Xu, H. Optical Forces on Interacting Plasmonic Nanoparticles in a Focused Gaussian Beam. *Phys. Rev. B* **2008**, *77*, 085412.
50. Chaumet, P. C.; Nieto-Vesperinas, M. Optical Binding of Particles with or without the Presence of a Flat Dielectric Surface. *Phys. Rev. B* **2001**, *64*, 035422.
51. Chu, P.; Mills, D. L. Laser-Induced Forces in Metallic Nanosystems: The Role of Plasmon Resonances. *Phys. Rev. Lett.* **2007**, *99*, 127401.
52. Chu, P.; Mills, D. L. Electromagnetic Response of Nanosphere Pairs: Collective Plasmon Resonances, Enhanced Fields, and Laser-Induced Forces. *Phys. Rev. B* **2008**, *77*, 045416.
53. Ng, J.; Tang, R.; Chan, C. T. Electrodynamics Study of Plasmonic Bonding and Antibonding Forces in a Bisphere. *Phys. Rev. B* **2008**, *77*, 195407.
54. Novotny, L.; Henkel, C. van der Waals *versus* Optical Interaction between Metal Nanoparticles. *Opt. Lett.* **2008**, *33*, 1029–1031.
55. Wong, V.; Ratner, M. A. Explicit Computation of Gradient and Nongradient Contributions to Optical Forces in the Discrete-Dipole Approximation. *J. Opt. Soc. Am. B* **2006**, *23*, 1801–1814.
56. Wong, V.; Ratner, M. A. Size Dependence of Gradient and Nongradient Optical Forces in Silver Nanoparticles. *J. Opt. Soc. Am. B* **2007**, *24*, 106–112.

57. Xu, H.; Käll, M. Surface-Plasmon-Enhanced Optical Forces in Silver Nanoaggregates. *Phys. Rev. Lett.* **2002**, *89*, 246802.
58. Burns, M. M.; Fournier, J. M.; Golovchenko, J. A. Optical Binding. *Phys. Rev. Lett.* **1989**, *63*, 1233–1236.
59. Burns, M. M.; Fournier, J. M.; Golovchenko, J. A. Optical Matter: Crystallization and Binding in Intense Optical-Fields. *Science* **1990**, *249*, 749–754.
60. Kyrsting, A.; Bendix, P. M.; Oddershede, L. B. Mapping 3D Focal Intensity Exposes the Stable Trapping Positions of Single Nanoparticles. *Nano Lett.* **2013**, *13*, 31–35.
61. Reihani, S. N. S.; Charsooghi, M. A.; Khalesifard, H. R.; Golestanian, R. Efficient in-Depth Trapping with an Oil-Immersion Objective Lens. *Opt. Lett.* **2006**, *31*, 766–768.
62. Hajizadeh, F.; Reihani, S. N. S. Optimized Optical Trapping of Gold Nanoparticles. *Opt. Express* **2010**, *18*, 551–559.
63. Bosanac, L.; Aabo, T.; Bendix, P. M.; Oddershede, L. B. Efficient Optical Trapping and Visualization of Silver Nanoparticles. *Nano Lett.* **2008**, *8*, 1486–1491.
64. Reihani, S. N. S.; Oddershede, L. B. Optimizing Immersion Media Refractive Index Improves Optical Trapping by Compensating Spherical Aberrations. *Opt. Lett.* **2007**, *32*, 1998–2000.
65. Balijepalli, A.; Gorman, J. J.; Gupta, S. K.; LeBrun, T. W. Significantly Improved Trapping Lifetime of Nanoparticles in an Optical Trap Using Feedback Control. *Nano Lett.* **2012**, *12*, 2347–2351.
66. Li, T. C.; Kheifets, S.; Medellin, D.; Raizen, M. G. Measurement of the Instantaneous Velocity of a Brownian Particle. *Science* **2010**, *328*, 1673–1675.
67. Harada, Y.; Asakura, T. Radiation Forces on a Dielectric Sphere in the Rayleigh Scattering Regime. *Opt. Commun.* **1996**, *124*, 529–541.
68. Nieminen, T. A.; Loke, V. L. Y.; Stilgoe, A. B.; Knoner, G.; Branczyk, A. M.; Heckenberg, N. R.; Rubinsztein-Dunlop, H. Optical Tweezers Computational Toolbox. *J. Opt. A: Pure Appl. Opt.* **2007**, *9*, S196–S203.
69. Seol, Y.; Carpenter, A. E.; Perkins, T. T. Gold Nanoparticles: Enhanced Optical Trapping and Sensitivity Coupled with Significant Heating. *Opt. Lett.* **2006**, *31*, 2429–2431.
70. Saija, R.; Denti, P.; Borghese, F.; Maragò, O. M.; Iatì, M. A. Optical Trapping Calculations for Metal Nanoparticles. Comparison with Experimental Data for Au and Ag Spheres. *Opt. Express* **2009**, *17*, 10231–10241.
71. Selhuber-Unkel, C.; Zins, I.; Schubert, O.; Sönnichsen, C.; Oddershede, L. B. Quantitative Optical Trapping of Single Gold Nanorods. *Nano Lett.* **2008**, *8*, 2998–3003.
72. Yan, Z.; Pelton, M.; Vigderman, L.; Zubarev, E. R.; Scherer, N. F. Why Single-Beam Optical Tweezers Trap Gold Nanowires in Three Dimensions. *ACS Nano* **2013**, *7*, 8794–8800.
73. Trojek, J.; Chavátal, L.; Zemánek, P. Optical Alignment and Confinement of an Ellipsoidal Nanorod in Optical Tweezers: A Theoretical Study. *J. Opt. Soc. Am. A* **2012**, *29*, 1224–1236.
74. Ruijgrok, P. V.; Verhart, N. R.; Zijlstra, P.; Tchebotareva, A. L.; Orrit, M. Brownian Fluctuations and Heating of an Optically Aligned Gold Nanorod. *Phys. Rev. Lett.* **2011**, 107.
75. Liu, Q. K.; Asavei, T.; Lee, T.; Rubinsztein-Dunlop, H.; He, S. L.; Smalyukh, I. I. Measurement of Viscosity of Lyotropic Liquid Crystals by Means of Rotating Laser-Trapped Microparticles. *Opt. Express* **2011**, *19*, 25134–25143.
76. Friese, M. E. J.; Enger, J.; Rubinsztein-Dunlop, H.; Heckenberg, N. R. Optical Angular-Momentum Transfer to Trapped Absorbing Particles. *Phys. Rev. A* **1996**, *54*, 1593–1596.
77. Friese, M. E. J.; Nieminen, T. A.; Heckenberg, N. R.; Rubinsztein-Dunlop, H. Optical Alignment and Spinning of Laser-Trapped Microscopic Particles. *Nature* **1998**, *394*, 348–350.
78. Jones, P. H.; Palmisano, F.; Bonaccorso, F.; Gucciardi, P. G.; Calogero, G.; Ferrari, A. C.; Maragò, O. M. Rotation Detection in Light-Driven Nanorotors. *ACS Nano* **2009**, *3*, 3077–3084.
79. Messina, E.; Cavallaro, E.; Cacciola, A.; Iatì, M. A.; Gucciardi, P. G.; Borghese, F.; Denti, P.; Saija, R.; Compagnini, G.; Meneghetti, M.; et al. Plasmon-Enhanced Optical Trapping of Gold Nanoaggregates with Selected Optical Properties. *ACS Nano* **2011**, *5*, 905–913.
80. Messina, E.; Cavallaro, E.; Cacciola, A.; Saija, R.; Borghese, F.; Denti, P.; Fazio, B.; D'Andrea, C.; Gucciardi, P. G.; Iati, M. A.; et al. Manipulation and Raman Spectroscopy with Optically Trapped Metal Nanoparticles Obtained by Pulsed Laser Ablation in Liquids. *J. Phys. Chem. C* **2011**, *115*, 5115–5122.
81. Liu, M.; Zentgraf, T.; Liu, Y.; Bartal, G.; Zhang, X. Light-Driven Nanoscale Plasmonic Motors. *Nat. Nanotechnol.* **2010**, *5*, 570–573.
82. Padgett, M.; Bowman, R. Tweezers with a Twist. *Nat. Photonics* **2011**, *5*, 343–348.
83. Dienerowitz, M.; Mazilu, M.; Reece, P. J.; Krauss, T. F.; Dholakia, K. Optical Vortex Trap for Resonant Confinement of Metal Nanoparticles. *Opt. Express* **2008**, *16*, 4991–4999.
84. Ito, S.; Yamauchi, H.; Tamura, M.; Hidaka, S.; Hattori, H.; Hamada, T.; Nishida, K.; Tokonami, S.; Itoh, T.; Miyasaka, H.; et al. Selective Optical Assembly of Highly Uniform Nanoparticles by Doughnut-Shaped Beams. *Sci. Rep.* **2013**, *3*, 3047.
85. Yan, Z.; Jureller, J. E.; Sweet, J.; Guffey, M. J.; Pelton, M.; Scherer, N. F. Three-Dimensional Optical Trapping and Manipulation of Single Silver Nanowires. *Nano Lett.* **2012**, *12*, 5155–5161.
86. Zhan, Q. Trapping Metallic Rayleigh Particles with Radial Polarization. *Opt. Express* **2004**, *12*, 3377–3382.
87. Iglesias, I.; Sáenz, J. J. Light Spin Forces in Optical Traps: Comment on "Trapping Metallic Rayleigh Particles with Radial Polarization". *Opt. Express* **2012**, *20*, 2832–2834.
88. Wang, L. G. Optical Forces on Submicron Particles Induced by Full Poincare Beams. *Opt. Express* **2012**, *20*, 20814–20826.
89. Marqués, M. I. Beam Configuration Proposal To Verify That Scattering Forces Come from the Orbital Part of the Poynting Vector. *Opt. Lett.* **2014**, *39*, 5122–5125.
90. Yan, Z.; Scherer, N. F. Optical Vortex Induced Rotation of Silver Nanowires. *J. Phys. Chem. Lett.* **2013**, *4*, 2937–2942.
91. O'Neil, A. T.; Padgett, M. J. Three-Dimensional Optical Confinement of Micron-Sized Metal Particles and the Decoupling of the Spin and Orbital Angular Momentum with an Optical Spanner. *Opt. Commun.* **2000**, *185*, 139–143.
92. Lehmuskero, A.; Li, Y. M.; Johansson, P.; Käll, M. Plasmonic Particles Set into Fast Orbital Motion by an Optical Vortex Beam. *Opt. Express* **2014**, *22*, 4349–4356.
93. Jiang, Y.; Narushima, T.; Okamoto, H. Nonlinear Optical Effects in Trapping Nanoparticles with Femtosecond Pulses. *Nat. Phys.* **2010**, *6*, 1005–1009.
94. Ng, L. N.; Zervas, M. N.; Wilkinson, J. S.; Luff, B. J. Manipulation of Colloidal Gold Nanoparticles in the Evanescent Field of a Channel Waveguide. *Appl. Phys. Lett.* **2000**, *76*, 1993–1995.
95. Gaugiran, S.; Gétin, S.; Fedeli, J. M.; Derouard, J. Polarization and Particle Size Dependence of Radiative Forces on Small Metallic Particles in Evanescent Optical Fields. Evidences for Either Repulsive or Attractive Gradient Forces. *Opt. Express* **2007**, *15*, 8146–8156.
96. Wang, K.; Schonbrun, E.; Crozier, K. B. Propulsion of Gold Nanoparticles with Surface Plasmon Polaritons: Evidence of Enhanced Optical Force from Near-Field Coupling between Gold Particle and Gold Film. *Nano Lett.* **2009**, *9*, 2623–2629.
97. Yang, A. H. J.; Lerdsuchatawanich, T.; Erickson, D. Forces and Transport Velocities for a Particle in a Slot Waveguide. *Nano Lett.* **2009**, *9*, 1182–1188.
98. Zhang, W.; Huang, L.; Santschi, C.; Martin, O. J. F. Trapping and Sensing 10 nm Metal Nanoparticles Using Plasmonic Dipole Antennas. *Nano Lett.* **2010**, *10*, 1006–1011.
99. Grigorenko, A. N.; Roberts, N. W.; Dickinson, M. R.; Zhang, Y. Nanometric Optical Tweezers Based on Nanostructured Substrates. *Nat. Photonics* **2008**, *2*, 365–370.

100. Berthelot, J.; Aćimović, S. S.; Juan, M. L.; Kreuzer, M. P.; Renger, J.; Quidant, R. Three-Dimensional Manipulation with Scanning Near-Field Optical Nanotweezers. *Nat. Nanotechnol.* **2014**, *9*, 295–299.
101. Demergis, V.; Florin, E. L. Ultrastrong Optical Binding of Metallic Nanoparticles. *Nano Lett.* **2012**, *12*, 5756–5760.
102. Lyklema, J.; van Leeuwen, H. P.; Minor, M. DLVO-Theory, a Dynamic Re-interpretation. *Adv. Colloid Interface Sci.* **1999**, *83*, 33–69.
103. Ling, L.; Huang, L.; Fu, J.; Guo, H.; Li, J.; Ou-Yang, H. D.; Li, Z.-Y. The Properties of Gold Nanospheres Studied with Dark Field Optical Trapping. *Opt. Express* **2013**, *21*, 6618–6624.
104. Svedberg, F.; Käll, M. On the Importance of Optical Forces in Surface-Enhanced Raman Scattering (SERS). *Faraday Discuss.* **2006**, *132*, 35–44.
105. Gunnarsson, L.; Rindzevicius, T.; Prikulis, J.; Kasemo, B.; Käll, M.; Zou, S. L.; Schatz, G. C. Confined Plasmons in Nanofabricated Single Silver Particle Pairs: Experimental Observations of Strong Interparticle Interactions. *J. Phys. Chem. B* **2005**, *109*, 1079–1087.
106. Sönnichsen, C.; Reinhard, B. M.; Liphardt, J.; Alivisatos, A. P. A Molecular Ruler Based on Plasmon Coupling of Single Gold and Silver Nanoparticles. *Nat. Biotechnol.* **2005**, *23*, 741–745.
107. Tong, L.; Righini, M.; Gonzalez, M. U.; Quidant, R.; Käll, M. Optical Aggregation of Metal Nanoparticles in a Microfluidic Channel for Surface-Enhanced Raman Scattering Analysis. *Lab Chip* **2009**, *9*, 193–195.
108. Tanaka, Y.; Yoshikawa, H.; Itoh, T.; Ishikawa, M. Laser-Induced Self-Assembly of Silver Nanoparticles *via* Plasmonic Interactions. *Opt. Express* **2009**, *17*, 18760–18767.
109. Tanaka, Y.; Yoshikawa, H.; Itoh, T.; Ishikawa, M. Surface Enhanced Raman Scattering from Pseudoisocyanine on Ag Nanoaggregates Produced by Optical Trapping with a Linearly Polarized Laser Beam. *J. Phys. Chem. C* **2009**, *113*, 11856–11860.
110. Yoshikawa, H.; Matsui, T.; Masuhara, H. Reversible Assembly of Gold Nanoparticles Confined in an Optical Microcage. *Phys. Rev. E* **2004**, *70*, 061406.
111. Königer, A.; Köhler, W. Optical Funneling and Trapping of Gold Colloids in Convergent Laser Beams. *ACS Nano* **2012**, *6*, 4400–4409.
112. Zhang, Y.; Gu, C.; Schwartzberg, M. A.; Chen, S.; Zhang, J. Z. Optical Trapping and Light-Induced Agglomeration of Gold Nanoparticle Aggregates. *Phys. Rev. B* **2006**, *73*, 165405.
113. Iida, T. Control of Plasmonic Superradiance in Metallic Nanoparticle Assembly by Light-Induced Force and Fluctuations. *J. Phys. Chem. Lett.* **2012**, *3*, 332–336.
114. Balint, S.; Kreuzer, M. P.; Rao, S.; Badenes, G.; Miskovsky, P.; Petrov, D. Simple Route for Preparing Optically Trappable Probes for Surface-Enhanced Raman Scattering. *J. Phys. Chem. C* **2009**, *113*, 17724–17729.
115. Tong, L. M.; Xu, H. X.; Käll, M. Nanogaps for SERS Applications. *MRS Bull.* **2014**, *39*, 163–168.
116. Lin, S.; Zhu, W.; Jin, Y.; Crozier, K. B. Surface-Enhanced Raman Scattering with Ag Nanoparticles Optically Trapped by a Photonic Crystal Cavity. *Nano Lett.* **2013**, *13*, 559–563.
117. Guffey, M. J.; Scherer, N. F. All-Optical Patterning of Au Nanoparticles on Surfaces Using Optical Traps. *Nano Lett.* **2010**, *10*, 4302–4308.
118. Nedev, S.; Urban, A. S.; Lutich, A. A.; Feldmann, J. Optical Force Stamping Lithography. *Nano Lett.* **2011**, *11*, 5066–5070.
119. Urban, A. S.; Lutich, A. A.; Stefani, F. D.; Feldmann, J. Laser Printing Single Gold Nanoparticles. *Nano Lett.* **2010**, *10*, 4794–4798.
120. Bao, Y.; Yan, Z.; Scherer, N. F. Optical Printing of Electrodynamically Coupled Metallic Nanoparticle Arrays. *J. Phys. Chem. C* **2014**, *118*, 19315–19321.
121. Do, J.; Fedoruk, M.; Jäckel, F.; Feldmann, J. Two-Color Laser Printing of Individual Gold Nanorods. *Nano Lett.* **2013**, *13*, 4166–4168.
122. Ploschner, M.; Čižmár, T.; Mazilu, M.; Falco, A. D.; Dholakia, K. Bidirectional Optical Sorting of Gold Nanoparticles. *Nano Lett.* **2012**, *12*, 1923–1927.
123. Zelenina, A. S.; Quidant, R.; Badenes, G.; Nieto-Vesperinas, M. Tunable Optical Sorting and Manipulation of Nanoparticles *via* Plasmon Excitation. *Opt. Lett.* **2006**, *31*, 2054–2056.
124. Guffey, M. J.; Miller, R. L.; Gray, S. K.; Scherer, N. F. Plasmon-Driven Selective Deposition of Au Bipyramidal Nanoparticles. *Nano Lett.* **2011**, *11*, 4058–4066.
125. Bendix, P. M.; Nader, S.; Reihani, S.; Oddershede, L. B. Direct Measurements of Heating by Electromagnetically Trapped Gold Nanoparticles on Supported Lipid Bilayers. *ACS Nano* **2010**, *4*, 2256–2262.
126. Kyrsting, A.; Bendix, P. M.; Stamou, D. G.; Oddershede, L. B. Heat Profiling of Three-Dimensionally Optically Trapped Gold Nanoparticles Using Vesicle Cargo Release. *Nano Lett.* **2011**, *11*, 888–892.
127. Urban, A. S.; Fedoruk, M.; Horton, M. R.; Rädler, J. O.; Stefani, F. D.; Feldmann, J. Controlled Nanometric Phase Transitions of Phospholipid Membranes by Plasmonic Heating of Single Gold Nanoparticles. *Nano Lett.* **2009**, *9*, 2903–2908.
128. Osinkina, L.; Carretero-Palacios, S.; Stehr, J.; Lutich, A. A.; Jäckel, F.; Feldmann, J. Tuning DNA Binding Kinetics in an Optical Trap by Plasmonic Nanoparticle Heating. *Nano Lett.* **2013**, *13*, 3140–3144.
129. Ni, W.; Ba, H.; Lutich, A. A.; Jäckel, F.; Feldmann, J. Enhancing Single-Nanoparticle Surface-Chemistry by Plasmonic Overheating in an Optical Trap. *Nano Lett.* **2012**, *12*, 4647–4650.
130. Arita, Y.; Ploschner, M.; Antkowiak, M.; Gunn-Moore, F.; Dholakia, K. Laser-Induced Breakdown of an Optically Trapped Gold Nanoparticle for Single Cell Transfection. *Opt. Lett.* **2013**, *38*, 3402–3405.
131. Fedoruk, M.; Meixner, M.; Carretero-Palacios, S.; Lohmuller, T.; Feldmann, J. Nanolithography by Plasmonic Heating and Optical Manipulation of Gold Nanoparticles. *ACS Nano* **2013**, *7*, 7648–7653.
132. Fedoruk, M.; Lutich, A. A.; Feldmann, J. Subdiffraction-Limited Milling by an Optically Driven Single Gold Nanoparticle. *ACS Nano* **2011**, *5*, 7377–7382.
133. Li, M.; Lohmüller, T.; Feldmann, J. Optical Injection of Gold Nanoparticles into Living Cells. *Nano Lett.* **2015**, *15*, 770–775.